ACOUSTIC NOISE

I. Dyer, Marblehead, MA, USA

doi:10.1006/rwos.2001.0315

Introduction

Some ocean scientists consider ambient noise to be a fairly simple and well-behaved property of the ocean. Ambient noise, after all, is often reported and summarized in highly averaged form, its naturally large variance mostly unstated. Other ocean scientists consider the variational complexity of ambient noise a richly colored portrait carrying images of basic ocean processes, including the physics of various noise sources and the acoustics of multiple noise propagation paths. Space and incomplete knowledge precludes a description here that can fully satisfy all ocean scientists or technologists. Instead, the objective is to summarize those aspects of ocean ambient noise that convey the more important recent research results and the more significant remaining research questions.

A 1962 summary of ambient noise measurements in the ocean (see **Figure 1**) is still useful today, at least to classify the various noise sources and their average levels and smooth frequency spectra. Prevailing noises (those observed almost always) are caused by wave–wave interactions at the sea surface, by distributed seismic activity in the earth, by atmospheric or oceanic turbulence, by distant shipping, by wind-induced sea surface agitation, and by thermally induced molecular agitation. According to Wenz, wave–wave interaction effects, seismic background, and/or turbulence dominates the noise at VLF (very low frequency band: $1 < f < 20$ Hz), with power spectral density of the pressure field $S(f) \propto f^{-4}$. Distant shipping noise dominates at LF (low frequency band: $20 < f < 200$ Hz), has a broad spectral peak around 50 Hz, and falls off sharply for $f > 200$ Hz as f^{-6}. At MF (midfrequency band: $200\,\text{Hz} < f < 50\,\text{kHz}$), noise caused by sea surface agitation typically dominates, with a broad peak within $200\,\text{Hz} < f < 2\,\text{kHz}$ and, beyond $f \approx 2$ kHz, with $S(f) \propto f^{-1.7}$. Finally, molecular agitation typically dominates the noise at HF (high frequency band: $f > 100$ kHz), with $S(f) \propto f^2$.

Other noise sources are classified as temporally intermittent or spatially discrete, rather than prevailing, and can often dominate. These include sounds from marine earthquakes, from marine animals, from nearby ships or other nearby commercial activities in the ocean, from rain/hail/snow striking the sea surface, and from fractures of ice in the north or south polar oceans. With such a large number of prevailing and other noise sources, the band designations given in the previous paragraph are unlikely to be associated unequivocally with just one noise source or, for that matter, adopted fully by most ambient noise researchers or practitioners. They are of use, however, to help present the material to follow.

The spectral summaries used in this Introduction are based on Wenz, and although still useful, modifications and additions are needed in the light of new knowledge. Urick published an excellent summary of ambient noise data acquired in various measurement programs through about 1980. Practitioners commonly use these data, plus the Wenz results, for prediction. Nevertheless, basic understanding of many ambient noise mechanisms through about 1980 was meager and, indeed, some suggested mechanisms were considered speculative. Fortunately, mechanisms for prevailing ambient noises have received considerable research attention since then, particularly from 1985 or so. The other noises have also been researched, in general to a lesser degree. Two volumes edited by Kerman and one by Buckingham and Potter are conference proceedings of recent ambient noise research, and are extraordinary seminal contributions to the understanding of ambient noise mechanisms in the ocean. The continuing flow of research results in archival journals and books, and the aforementioned volumes, provide important modifications and additions to the classical summary of ambient noise by Wenz. In what follows the more important new knowledge, or lack thereof, is summarized.

ULF Band: Wave–Wave Interaction Noise

Measurements within $0.1 < f < 2$ Hz, which has come to be called the ultralow frequency band (ULF), extended the Wenzian picture one decade lower in frequency[1], and showed ULF noise to be a function of wind speed. The data (**Figure 2**), have a strong peak f_0 located between about 0.2 and 0.7 Hz, with $S(f)$ at higher f proportional to about f^{-3}–f^{-5}, dependent upon wind speed. A long

[1] To accommodate the ULF band, the band scheme described in the Introduction is redefined to be VLF = 2–20 Hz.

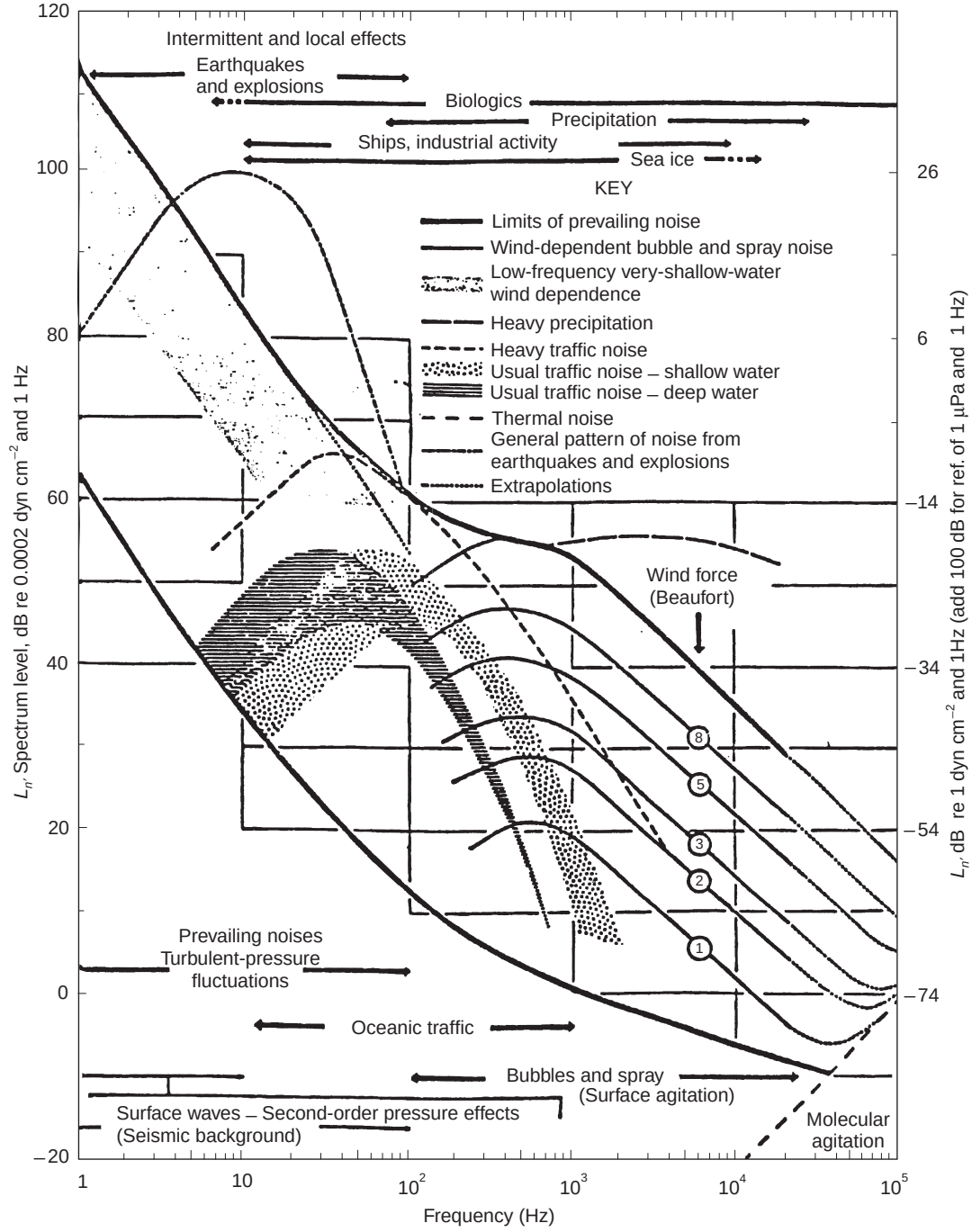

Figure 1 Ambient noise spectra summarized by Wenz. (The ordinates are $L_n = 10 \log_{10} S(f)$, with respect to the reference value. Add 100 dB to the right-hand scale to obtain L_n in dB re 1 μPa and 1 Hz.) The Beaufort Force translates to wind speeds, in ms $^{-1}$, as follows: 1, 0.5–1.5; 2, 2–3; 3, 3.5–5; 5, 8.5–10.5; 8, 17–20. (Reproduced from Wenz, 1962.)

history of measurements, as well as theoretical surface wave interaction studies, presaged this result. The appearance of systematic data such as in **Figure 2** apparently sparked even more research efforts that ultimately confirmed the basic aspects of ULF noise.

Pressure Spectral Density

Wave–wave interaction noise is caused by opposing wind-driven surface gravity waves, each at frequency f_w, that to second-order create a pressure field in the water at $f = 2f_w$. (Orders higher than the

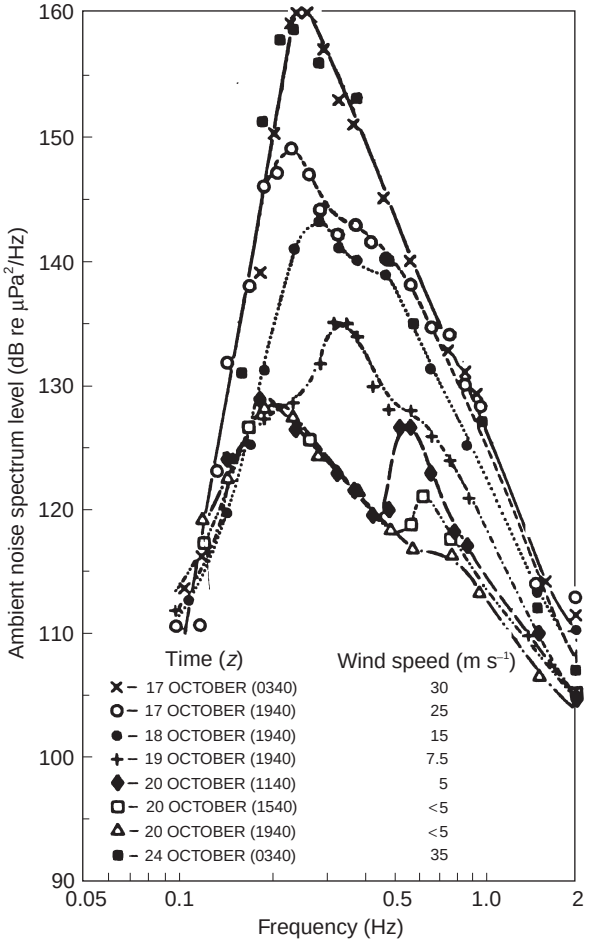

Figure 2 Ambient noise pressure derived from vertical displacement (seismometer) data at the water/bottom interface (depth about 100 m). (Reproduced from Kibblewhite and Evans, 1985.)

second have been shown to be negligible.) In its simplest form, the spectral density S of the pressure field is

$$S(f,z) = (\pi^3\rho^2\boldsymbol{g}^2/2c^2)[S_w(f/2)]^2 f^3 \Phi(f/2) T_p(f,z) \qquad [1]$$

where ρ is water density, c is water sound speed, $\boldsymbol{g}$ is acceleration of gravity, S_w is the spectral density of the surface wave elevation, Φ is an integral over all azimuth angles ϕ of the product of the normalized azimuthal directivity of the opposing surface waves (for ϕ and $\phi + \pi$), and T_p is a function normalized by its value at depth $z = 0$ that relates the pressure spectral density at the surface to that at z, which importantly includes acoustic coupling to the sea bottom. For simplicity, eqn [1] includes contributions to the noise field only for horizontal phase speeds given by $c_x \geq c$. Because of its exponential decay in z, the remaining regime $c_x < c$ is important mostly for depths approaching $z = 0$, especially for lower f, and is included in fuller analyses.

The noise spectral density $S(f)$ is proportional to $[S_w(f/2)]^2$, the surface elevation density squared and shifted in frequency. Since the frequency dependence of the last three terms in eqn [1] is relatively weak around the peak frequency f_{wo} of S_w, the peak of S is essentially $f_o \approx 2f_{wo}$. Both f_{wo} and S_w are functions of wind speed U, as affected by other sea conditions (fetch, sea age, etc.), and similarly lead to the dependence of f_o and S on U.

Microseism Spectral Density

Displacement, rather than pressure, is often measured on the seafloor. Termed microseism noise, it can be obtained from eqn [1] with the substitution of a modified transfer function $T_d(f,z)$ for $T_p(f,z)$, each in general given for all z, to yield the displacement spectral density $S_d(f,z)$ rather than $S(f,z)$. These transfer functions incorporate the acoustics of the medium, including the seismoacoustics of the bottom. It is no surprise, therefore, that noise pressure or displacement data may show subsidiary peaks in the frequency domain, additional to the major peak at f_o, associated with acoustic modes of the oceanic waveguide.

With modifications as outlined in the foregoing and as detailed in the literature, and with site-specific seismic–acoustic bottom properties and time- and site-specific sea surface elevations, data such as in **Figure 2** are remarkably well predicted with use of the theory symbolized by eqn [1]. The theory may also be extended to cover interaction of swells with wind waves, with use of $S_w S_s$ instead of S_w^2, where S_s is the swell spectral density, and with Φ similarly including the swell azimuthal directivity.

VLF Band: Atmospheric Turbulence Forcing as a Noise Source

The heading of this section is in reality a question. In the VLF band (2–20 Hz), and to somewhat higher frequencies in seas with very low shipping density, noise measurements do not match direct extrapolation of wave–wave interaction data as in **Figure 2**. Other mechanisms may become important in this band, and one has attracted considerable attention, namely turbulent pressure fluctuations in the atmosphere that drive the ocean surface. Is the latter the responsible mechanism? And if not, what is? A robust answer is not yet available.

In one of the more extensive data summaries dating from the 1960s, Crouch and Burt showed

that in the absence of shipping noise, and at low wind speeds, S is $\propto f^{-1}U^0$ between about 10–50 Hz. This holds until a crossover wind speed U_c is reached ($\approx 16\,\mathrm{m\,s^{-1}}$ at 11 Hz), beyond which S is roughly $\propto f^{-3}U^4$. The crossover speed U_c tends to increase with increasing frequency up to about 50 Hz.

Nichols reported some data that also included frequencies lower than those of Crouch/Burt. These data show that for a small spread of wind speeds around $U \approx 9\,\mathrm{m\,s^{-1}}$, $S \propto f^{-2.5}$ from 3 to 8 Hz, and $S \propto f^0$ from 8 to 20 Hz. These results compare well with those of Crouch/Burt at the overlapping frequencies, and add a functional form below 8 Hz not covered by Crouch/Burt. Nichols also summarized unpublished data for U varying from about 3 to $9\,\mathrm{m\,s^{-1}}$, that show $S \propto f^{-5}U^5$ from 2 to 5 Hz, and $S \propto f^0U^5$ from 5 to 10 Hz. (The f^0U^5 functional form could be argued from the data shown to be f^0U^0 at lower U, and $f^0U^{>5}$ at higher U.) This form at the lowest frequencies has a much sharper falloff with frequency than the Nichols' form, but preference should be given to it because the frequency resolution was much finer. Accordingly, the overall result, labeled 'Nichols', is stated here as $S \propto f^{-5}U^5$ from 2 to 5 Hz, and f^0U^5 from 5 to 20 Hz.

More recently, as part of LF noise measurement programs, data in the upper part of the VLF band were published. Deep ocean noise versus U at $f = 13$ and 50 Hz has been reported. For $5 \le U \le 15\,\mathrm{m\,s^{-1}}$, these data have a functional form approximately $S \propto f^{-0.8}U^{1.3}$ (perhaps more like $f^0U^{1.6}$ at the highest U). A report of shallow water noise versus U in third-octave bands for $10 \le f \le 20$ Hz, with form $S \propto f^{-3.2}U^{3.4}$ for $U = 3$ and $5\,\mathrm{m\,s^{-1}}$ in late fall, had data that differed so widely for $U = 5$ and $9\,\mathrm{m\,s^{-1}}$ in late spring that a functional form could not be stated. One report of deep ocean noise at $f = 15$ and 25 Hz, for $2 \le U \le 12\,\mathrm{m\,s^{-1}}$, suggests $S \propto f^0U^{-0.5}$ for $U < U_c$, and $S \propto f^0U^3$ for $U > U_c$, with the crossover speed $U_c \approx 8\,\mathrm{m\,s^{-1}}$.

What noise mechanism could account for all the foregoing observations? An extrapolation of wave–wave interaction noise to the VLF band, from data such as in **Figure 2**, suggests that $S \propto f^{-4}U^{1/2}$, give or take one integer in the exponent of f, and one-half integer in the exponent of U. However, this is unacceptably far from the data. The Crouch/Burt data suggest $f^{-1}U^0$ and $f^{-3}U^4$ for low and high U, respectively. The overall Nichols result is $f^{-5}U^5$ from 2 to 5 Hz, and f^0U^5 from 5 to 20 Hz. Other data give $f^{-0.8}U^{1.3}$, $f^{-3.2}U^{3.4}$ or an indefinite form, and $f^0U^{-0.5}$ and f^0U^3 for low and high U, respectively. Without significant modifications applicable to the VLF band, it seems that the wave–wave interaction possibility must be set aside.

Next, consider the atmospheric turbulence model. It has evolved as most theories do, but is contentious. It predicts $S \propto f^0U^4$. This, too, is mostly far from the functional form of the foregoing data, but does come close to Nichols and others (at the higher wind speeds) for the 5–25 Hz range. It seems inappropriate, however, to choose among available data sets for the ones that confirm a model. The difference between the data sets may well be caused by some mechanism that we are collectively ignorant of.

Finally, it is possible that available data are at least partially contaminated by hydrophone flow noise, whose functional form goes as f^{-4}. None of the data sets matches this form. Thus, it can be concluded that the hydrophone flow noise mechanism is an unlikely cause of VLF noise. The identification of the mechanism responsible for VLF noise can thus not be made with confidence.

In searching for candidate VLF noise mechanisms, one is inclined to look toward appropriate extensions or modifications of mechanisms in the adjacent ULF and LF bands, mainly because wave–wave interactions and distant shipping, respectively, are well established. Nonprevailing mechanisms should also be considered. For example, whale vocalizations are observed for $15 < f < 35$ Hz and can affect the VLF band.

Noise data sets beyond those referred to here, supported by environmental data as suggested by candidate mechanisms, may well be needed. The Crouch/Burt data set incorporated a plausible but convoluted data analysis path to extract the VLF noise. The reported database of Nichols is not large. The VLF data of other workers could have been affected, as the authors acknowledged, by distant shipping noise. Perhaps because many of these research efforts were aimed at other objectives, environmental data provided with the noise data are generally too fragmentary to aid the search for VLF mechanisms.

LF Band: Distant Shipping Noise

Evolving technology has altered the view of distant shipping noise. Increasing use of large aperture acoustic arrays, with attendant high-resolution beamwidths and focused scanning in range and use of high-resolution frequency filters, blurs the distinction once sharp between distant and local ships. That is, ambient noise at LF can be observed with high-resolution technology as a countable number

of discrete ship noise sources, rather than as a sum of noise from a very large number of widely distributed ships.

Frequency Spectra

Figure 3 shows the noise radiated by a contemporary cargo ship. The radiation is largely tonal, as has long been known. However, this is not obvious from the spectra shown in **Figure 1**, because they entail sums over many ships. The tonal envelopes in **Figure 3** maximize between about 20 and 80 Hz, in good agreement with the summation spectra shown in **Figure 1**. Acoustic propagation losses in the ocean change the shape of the source spectrum shown in **Figure 3**; above about 80 Hz, the spectrum observed distantly is increasingly reduced with increasing f and with increasing distance from the ship.

Directional Spectra

Noise radiated by a ship is a function of azimuth ϕ_s, and vertical angle θ_s, in a cylindrical coordinate system attached to the ship. The azimuthal spectral shape S_ϕ $(\phi; f, z)$ observed for a single ship at longer ranges is close to that measured near the ship. However, propagation of the noise to large ranges fundamentally affects the vertical directional spectrum $S_\theta(\theta; f, z)$. In these spectra, ϕ and θ are in a coordinate system attached to the observer ($\theta = 0$ is the local horizontal plane). **Figure 4** shows S_θ as measured in deep water by a vertical line array. It sums over the directional spectrum in azimuth S_ϕ, and therefore over the areal distribution of ships. A prominent feature of S_θ is a pedestal of high noise around the horizontal, which is weakly dependent on f and z, and varies in half-width θ_w from about ± 15 to 20°. These values are consistent with $\cos \theta_w \approx c_z/c_b$, where c_z and c_b are the sound speed at the observation depth and at the bottom, respectively. Distant shipping noise in deep water thus arrives mostly from source radiation at the surface near $|\theta_s| = 0$, and then propagates to the observer via refraction and surface reflection paths in the water. Bottom reflection or transmission losses are relatively high, so that these paths are less important. Other effects influence the pedestal including, but not limited to, surface waves that modulate the source amplitude, scattering rather than specular reflection from the rough sea surface, and scattering from a seamount or continental margin. Because of these oceanographic and topographical complexities, the shape of the noise pedestal in **Figure 4** is not general but instead suggestive of the main features of S_θ in the deep ocean.

In shallow waters, if $c_z/c_b > 1$ (downward refracting profile), then S_θ is governed by path or mode losses, including those attributable to the bottom. If

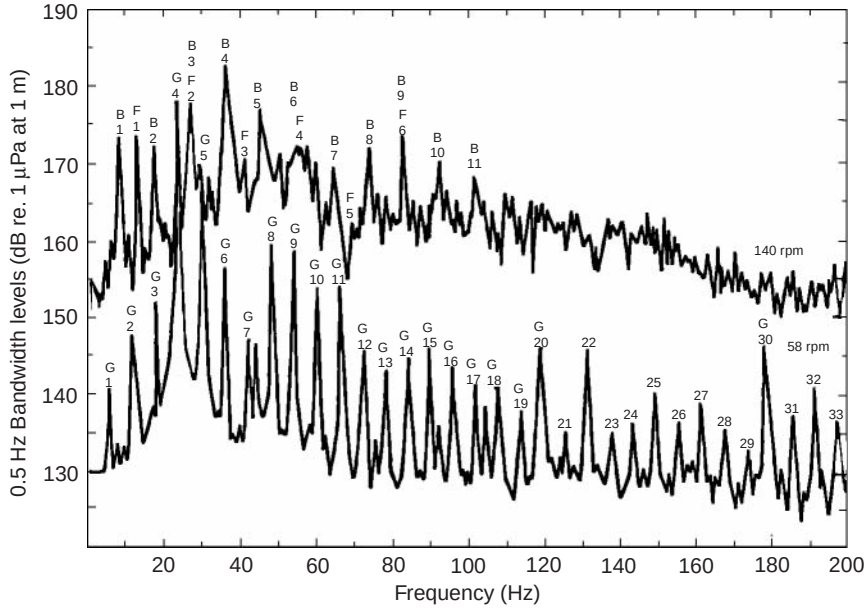

Figure 3 On-axis source level spectra of a cargo ship at 8 and 16 knots (4 and 8 m s^{-1}) measured directly below the ship. Noise levels at distances beyond 1 m may be obtained by subtracting the transmission loss. Levels for bandwidths other than 0.5 Hz can not be determined from this figure because the bandwidths of the tones are not given. (B, F, and G in the figure identify, respectively, the harmonics of the (propeller) blade rate, the (diesel engine) firing rate, and the (ship's service) generator rate.) (Reproduced from Arveson and Vendittis, 2000.)

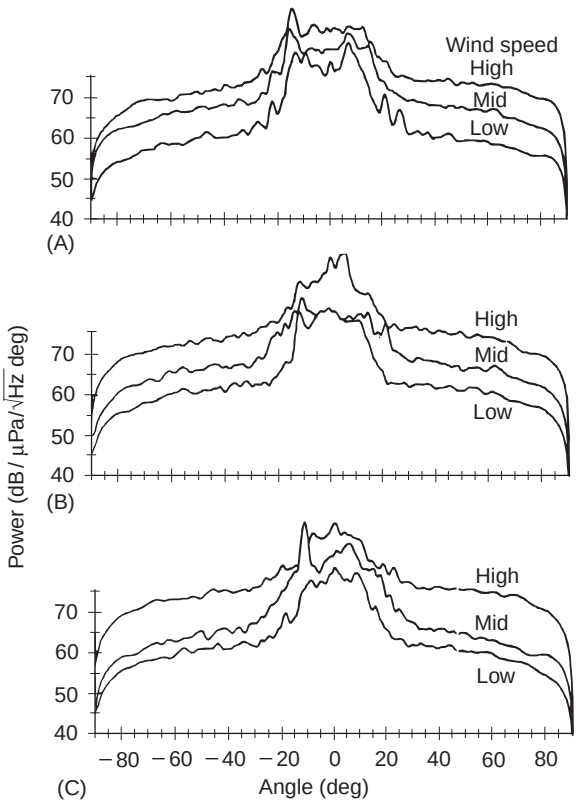

Figure 4 Vertical angle directional spectrum S_θ summed in azimuth in deep water for $f = 75$ Hz and $U = 3, 7$, and 11 m s^{-1}. Positive angles are upward looking. (A) Shallow, (B) mid, and (C) deep depth refers to the vertical line array (VLA) centered at z = 850, 1750, and 2650 m. The half-power beamwidth of the VLA at this frequency is about 1.3° when steered to $\theta = 0$. (Reproduced from Sotrin and Hodgkiss, 1990.)

$c_z/c_b < 1$ (upward refracting profile), then S_θ would have a pedestal, but with θ_w typically an order of magnitude smaller than that observed in the deep ocean.

Summation Issues

With several thousand ships underway in each of the heavily traveled oceans, taking account of all at the same time to determine distant shipping noise is neither feasible nor necessary. At one extreme, low-resolution data in the LF band (20–200 Hz) are relatively insensitive to the detailed noise source characteristics of individual ships. Because summation from a large number of ships merges the details, only the broad and slowly evolving trends in shipping lane location, in shipping density, and in shipping composition will affect the level and horizontal directionality of the noise. At the other extreme, high-resolution data resolve the frequency and spatial spectra associated with distant ships, thus giving the experimenter the *in situ* noise field in relevant detail. The experimenter can avoid such noise in the spectral valleys between tones or the spatial valleys between high-noise beams[2]. Aside from limits that may be imposed by the focusing, filtering, or beam-forming processor, the spectral valleys are set by the ship's radiation of continuous rather than tonal noise, and the spatial valleys by the sum of noise from more distant or less powerful ships. In addition, the valleys can be influenced by nonprevailing sources, the most prominent of which at LF is whale vocalization from about 15 to 35 Hz.

VLF Implications

With respect to the VLF band, the tonal envelope of a ship for $f < 20$ Hz, at all of its higher speeds is about f^0. Because very low frequency sounds can be detected at transoceanic distances, distant ships could cause the measured result to be $S \propto f^0 U^0$ found in some VLF experiments, in the apparent but not real absence of distant ships.

MF Band: Wind-driven Sea Surface Noise

Bubbles created by wind-driven surface waves have long been thought to be the dominant source of prevailing noise in the MF band (0.2–50 kHz). Many basic physical details, however, have only recently become better understood, and some relevant additional questions only recently posed. Various wave-breaking processes of wind-driven surface waves entrain air in the upper part of the ocean. Air-filled bubbles in the water are pinched off from the entrained air, which in turn oscillate and radiate noise as acoustic monopoles. Such noise thus entails wave-breaking and bubble hydrodynamics, both of which are addressed elsewhere in this encyclopedia. The acoustical aspects are addressed here.

Vertical Directional Spectrum

In its simplest form, the theory for noise generated by a uniform distribution of sources on the surface is, from ray acoustics,

$$S_\theta^+(\theta; f, z) = (c_s/c_z)\Sigma D\{\sin\theta_s(1 - R_b R_s)\}^{-1} \qquad \theta_w \le \theta \le \pi/2 \qquad [2]$$

$$S_\theta^-(\theta; f, z) = R_b S_\theta^+, \quad -\pi/2 \le \theta \le -\theta_w \qquad [3]$$

[2] Many ocean processes broaden tonal bandwidths and spatial beamwidths as the sound propagates from source to receiver. Such broadening is typically large enough to be a candidate ocean monitoring tool, but not so much that it completely fills the valleys.

where

$$\cos\theta_w = c_z/c_s \quad \text{for} \quad c_z/c_s < 1,$$

$$\text{or} \quad \theta_w = 0 \quad \text{for} \quad c_z/c_s > 1 \qquad [4]$$

and where the directional spectrum in vertical angle S_θ, per unit solid angle, is a function of f (at least through Σ, the pressure spectral density of the source per unit surface area) and of observation depth z (through sound speed c_z at z). The superscripts + and – refer to positive (upward looking) and negative (downward looking) θ obtained from $\cos\theta = (c_z/c_s)\cos\theta_s$ (the grazing angle θ_s and sound speed c_s pertain to $z = 0$). $D(\theta_s, f)$ is the directivity of the elemental bubble noise sources distributed just below the surface. For present purposes, the surface source distribution Σ, and the acoustic waveguide, is taken as uniform and independent of range and azimuth, contributions from propagation in the bottom are neglected, and volumetric absorption in the seawater is neglected. (These simplifications are adopted to keep the main ideas clear but, for more precise needs, can readily be replaced by assumptions that are more realistic.)

For a downward refracting sound speed profile to depth z ($c_z/c_s < 1$), the ray theory of eqns [2]–[4] predicts a refractive shadow zone or notch of width $2\theta_w$ around $\theta = 0$, the horizontal plane. Wave theory must be used to properly predict the field in the notch, which also can be partially filled by scattering of the noise from midwater depths by fish schools and by ocean inhomogeneities. For an upward refracting profile ($c_z/c_s > 1$), the field around $\theta = 0$ is directly due to the surface-generated noise, plus possible scattering contributions.

In eqns [2] and [3], R_b and R_s are, respectively, the coefficients of bottom and surface specular reflection. Terms involving these parameters can be important in the directional spectrum (but since perfect reflection is not likely for an acoustic waveguide in the ocean, they do not lead to singularities as eqns [2]–[4] might appear to suggest). For example, consider that R_b and R_s approach unity (but do not reach it) as the grazing angles at the bottom and the surface, respectively, approach zero. Then, for θ within about $\pm\pi/4$, S_θ can be increased in typical situations by about 10 dB. In addition, the bottom propagation paths neglected here can actually contribute, especially at the lower MF frequencies. Thus details of the acoustic waveguide affect S_θ^+ and S_θ^- and, along with the sound speed profile $c(z)$, could account for the plethora of somewhat dissimilar measured MF vertical directional spectra in the literature.

Eqn [2] contains the bubble source directivity $D(\theta_s, f)$ that, unfortunately, is not known with confidence. At least two models for directive radiation from aggregated bubbles have been considered. One assumes an exponential decrease of uncorrelated monopoles below a horizontal perfectly reflecting surface, and the other assumes a similarly situated monopole distribution concentrated on a submerged plane. Then, respectively,

$$D = 2\{1 - \text{sinc}(2k_s d\sin\theta_s)\} \qquad [5]$$

$$D = 4\sin^2(k_s d\sin\theta_s) \qquad [6]$$

where k_s is the acoustic wavenumber at the surface, d is the effective depth (the e-folding depth and the δ-function depth, respectively), and sinc $(x) \equiv (\sin x)/x$. In the limit $k_s d \sin\theta_s \ll 1$, these functions have the same shape, and close to the same magnitude (≈ 1 dB different). Data, however, show that the two are distinct. For eqn [5], the data suggest $k_s d \approx \pi$, whereas for eqn [6] $k_s d \approx \pi/2$. In either case, the idealized states assumed in eqns [5] and [6] might not represent the relevant complexity of the radiating bubbles beneath a breaking wave. For example, the exponential decay of bubble density with depth may well be a good model for horizontally isotropic bubbles quasistatically present as a result of previous wave breaking events, but a poor model for radiating bubbles immediately caused by a new event.

Integration of eqns [2]–[4] over θ to obtain the noise spectral density $S(f, z)$ also depends sensitively on R_b and R_s (and on possible bottom propagation paths). This emphasizes the need to compare experimentally derived values of $S(f, z)$ with appropriate knowledge of the acoustic waveguide. Alternatively, with use of eqns [2]–[4], Σ may be extracted from vertical line array (VLA) data. When a VLA is steered to $\theta = \pi/2$, the specular reflection and the bottom propagation paths will contribute at most weakly. Such a measurement is thus dominated by local surface sources, so that Σ may be compared among measurements with less concern for waveguide properties.

Source Spectral Density

Chapman and Cornish measured Σ in deep water with an upward-looking VLA. They apparently assumed eqn [6] for D, with $k_s d \approx \pi/2$. Their data at $f = 110$ Hz, and for the wind speed interval $2 < U < 15\,\text{m s}^{-1}$, are reproduced in **Figure 5**, and show a crossover wind speed $U_c \approx 4.3\,\text{m s}^{-1}$. The frequency interval for their measurements

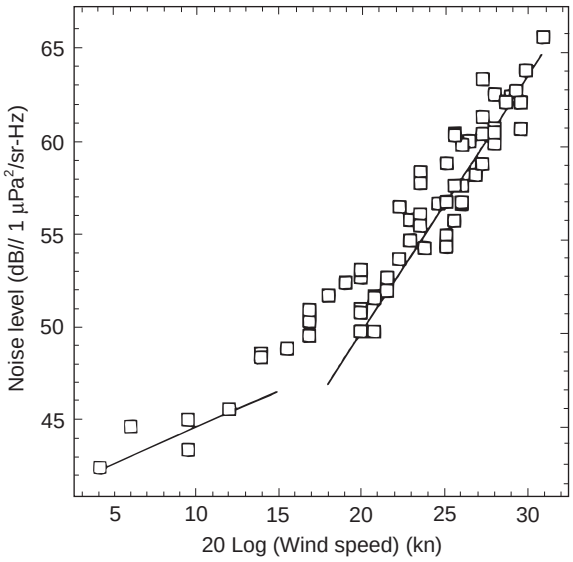

Figure 5 Level of the source spectral density Σ, in dB re μPa² per m² Hz, for $f = 110$ Hz. The 10 m wind speed U is in kn (1 kn ≈ 1/2 m s^{-1}). (Reproduced from Chapman and Cornish, 1993.)

is $13 < f < 300$ Hz, within which they found that U_c is about 4.3 m s^{-1} for $f \leq 110$ Hz, and that U_c is somewhat smaller (≈ 3.5 m s^{-1}) for $f > 110$ Hz. Chapman/Cornish attribute the crossover speed to a transition in source mechanism physics. Furthermore, by regression analyses, their data show that for $U < U_c$, $\Sigma \propto f^{-2.1}U^{0.6}$, and for $U > U_c$, $\Sigma \propto f^{-2.1}U^{2.7}$. These results hold on average within the speed and frequency intervals measured.

Kewley, Browning, and Carey reviewed and compared several data sets, mostly deep water VLA measurements, to extract Σ. They also used eqn [6] and $k_s d \approx \pi/2$, and concluded that for $30 < f < 1300$ Hz and $1 < U < 15$ m s^{-1}, $U_c \approx 6$ m s^{-1} with $\Sigma \propto U^1$ for $U < U_c$ and $\Sigma \propto U^3$ for $U > U_c$. The Kewley *et al.* wind speed exponents of 1 and 3 are not too different from those of Chapman/Cornish. When one considers that the former tilted their exponent choices somewhat to agree with extant physical models proposed for the below and above U_c regimes, the agreement can be considered quite satisfactory.[3] What is more relevant, however, is that a universal spectral shape is not evident for either regime in the Kewley *et al.* comparisons. More likely than not Σ, f, and D need to be scaled by hydrodynamic parameters other than or additional to U, as shown below.

[3] When compared at the same U and f, Σ is about 3 dB higher in the Chapman/Cornish data set than in the data reviewed by Kewley *et al.*

Basic Wave-Breaking Correlates

Research results on hydrodynamically based scaling of noise from breaking waves have been reported. Kerman has proposed that at $u_*/u_c \approx 1$, where u_* is the friction velocity and u_c is the minimum phase speed of gravity/capillary surface waves, the wave-breaking process transitions from one that has an aerodynamically smooth sea surface to another that is rough. Kennedy analyzed VLA data in a deep, acoustically isolated bay ($40 < f < 4000$ Hz, $2 < U < 15$ m s^{-1}), with unlimited wind fetch but limited wave fetch. It was found that $u_*/u_c > 0.9$ defined a rough surface regime. (It may therefore be presumed that the crossover speed discussed in the foregoing section is $U_c \approx 0.9\,u_c$.) **Figure 6** shows that the spectral data for $u_*/u_c > 0.9$ aggregate to an almost universal scalable spectrum. What garners the caveat of 'almost' is that frequency is scaled by f_p, the observed peak frequency. Both Kerman and Kennedy point out that f_p does not vary strongly. It ranges from about 300 to 800 Hz in the Kennedy data, and is not unlike that sketched by Wenz (**Figure 1**). But experimental interest does not always include measurement of f_p, in which case a user of **Figure 6** must slide the frequency scale without benefit of Kennedy's judgement. Neither, however, can properly be accused of intellectual sloth. Kerman provides a model for f_p, which contains wave-breaking parameters that unfortunately are poorly known. Kennedy's collapsed spectral spread although acceptably small, is large enough, and the frequency dependence for $1/3 < f/f_p < 10$ is weak enough, to forego fine attention to f_p. Although

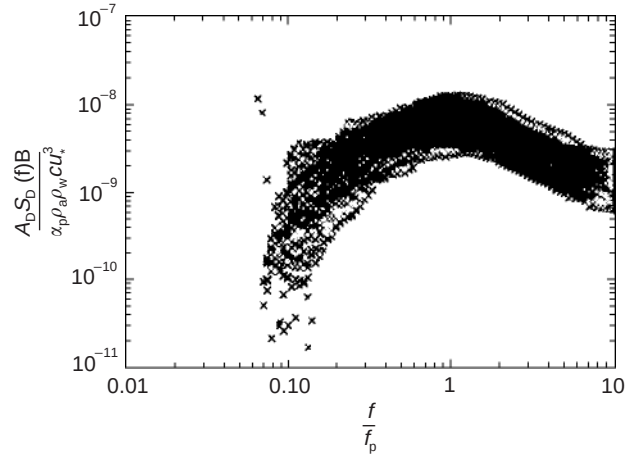

Figure 6 Source spectral density Σ versus f, both nondimensional as described in the text. The source directivity model used is presumably eqn [6] with $k_s d \ll 1$ (the compact dipole model). Data are for the aerodynamically rough regime ($u_* > u_c$). (Reproduced from Kennedy, 1992.)

apparently not used, f_p is related semi-empirically to breaking-wave whitecap size [f_p(in Hz) $\approx 1400/\sqrt{(LW)}$, where L and W are, respectively, the whitecap along-crest length and cross-crest width, both in meters].

The source spectral density Σ in **Figure 6** is obtained by Kennedy from a dipole directivity model. In effect, eqn [6] was used with $k_s d \ll 1$, in this limit known as a compact dipole. With this assumption, the integral of $D(f, \theta_s)$ over a hemispherical surface yields $A_D = 2\pi/3$, and this appears as one of the Σ scaling terms in **Figure 6**.[4] Another term is $B = 1000\,\text{Hz}$, the nominally observed bandwidth of the noise; its role is simply to create an integral measure ΣB for dimensional clarity. In the term $E = 5\rho_a u_*^3$, ρ_a is air density, and E is the major scaling variable, the average rate of energy dissipated per unit surface area by the breaking waves. Finally, $A_D \Sigma B/(\rho_w c_s)$, where ρ_w is water density, is the average rate of acoustic energy radiated per unit surface area.

Virtually simultaneously and independently, others have researched in greater depth some concepts that are related to the Kerman/Kennedy result. Noise spectral density $S(f, z)$ has been correlated with dissipation E, in deep water under steady wind and wave conditions, for the intervals $4.3 < f < 14\,\text{kHz}$ and $2 < U < 12\,\text{m s}^{-1}$. The data on average show $S \propto \Sigma \propto f^{-0.4} E^{0.74}$, with the exponent of E varying from 0.86 to 0.67 from the low to the high end of the frequency interval. At constant E, the frequency dependence agrees reasonably with an extrapolation of **Figure 6**. But the dissipation dependence can not be compared without scaling the peak frequency f_p, which was not observed. Thus, for a range of E one can seek the range of f_p to satisfy linear scaling in E. The peak frequency f_p would then need to decrease about a factor of 4 from low to high E, a factor so large as to suggest that a major change in noise physics occurs at these higher frequencies. Does the quasistatic bubble layer below the sea surface increasingly attenuate the noise, or increasingly inhibit its generation, at these frequencies? Bubbles are known to attenuate sound as a function of frequency and size distribution, but data analyses do not consider this.

With use of the Fresnel field of an array of hydrophones, sound radiated by individual breaking waves has been measured in deep water ($0.35 < f < 4\,\text{kHz}$, $4 < U < 15\,\text{m s}^{-1}$). The on-axis source levels of individual breaking events, were obtained and modeled as spatially and temporally discrete compact dipoles (eqn [6] with $k_s d \ll 1$). The individual source levels were correlated with U and c_b, the latter being the speed of a breaking wave event, a measure closely connected to breaking wave dissipation E. The correlation with c_b was found to be significantly better than that with U and, via physical arguments it was concluded that the source levels are well correlated with E. This measurement technique is also important as it determined the probability density of the dipole source levels, and the spatial density of discrete breaking wave events. It was also concluded, again via physical arguments, that the source spectral density for the frequencies measured are on average $\propto E^{0.83}$, which in view of the lower frequencies observed might be taken as reasonably consistent with the $E^{0.74}$ obtained by other workers. Thus the question remains on a possible frequency-dependent bubble layer effect.

The foregoing results clearly have not answered all questions on MF noise caused by breaking waves. They do, however, provide more general predictive tools than those previously available, and identify at least some of the more important physical attributes of noise from breaking waves.

HF Band: Molecular Noise

Molecules impinging on the surface of a pressure sensor cause noise, as estimated from physical principles and as plotted in **Figure 1**. Molecular motion, and thus momentum reversal on the sensor (i. e., force per unit area) is a function of molecular kinetic energy, and thus seawater temperature. On an absolute temperature scale, all oceans may be considered at a constant temperature. Hence, one line in **Figure 1** is sufficient to estimate the noise.

See also

Acoustics, Arctic. Acoustics, Deep Ocean. Acoustics, Shallow Water. Ships.

Further Reading

Arveson PT and Vendittis DJ (2000) Radiated noise characteristics of a modern cargo ship. *Journal of the Acoustical Society of America* 107: 118–129.

Buckingham MJ and Potter JR (eds) (1995) *Sea Surface Sound '94*, vol. 3. Singapore: World Scientific, 494pp.

Chapman NR and Cornish JW (1993) Wind dependence of deep ocean ambient noise at low frequencies. *Journal of the Acoustical Society of America* 93: 782–789.

[4] A spherical surface for the integral would seem more appropriate, since the only way a monopole can become a dipole is by including the negative image above the free surface, in which case $A_D = 4\pi/3$. Had a noncompact dipole been assumed with $k_s d = \pi/2$ (eqn [6]), then $A_D = 2\pi$. There is as much as 5 dB difference in these values compared to the one used by Kennedy.

Crouch WW and Burt PJ (1972) The logarithmic dependence of surface-generated ambient-sea-noise spectrum level on wind speed. *Journal of the Acoustical Society of America* 51: 1066–1072.

Kennedy RM (1992) Sea surface sound source dependence on wave-breaking variables. *Journal of the Acoustical Society of America* 91: 1974–1982.

Kerman BR (1984) Underwater sound generation by breaking wind waves. *Journal of the Acoustical Society of America* 75: 149–165.

Kerman BR (ed.) (1988) *Sea Surface Sound*, vol. 1. Dordrecht: Kluwer Academic Publishers, 639pp.

Kerman BR (ed.) (1993) *Sea Surface Sound*, vol. 2. Dordrecht: Kluwer Academic Publishers, 750pp.

Kewley DJ, Browning DG and Carey WM (1990) Low-frequency wind-generated ambient noise source levels. *Journal of the Acoustical Society of America* 88: 1894–1902.

Kibblewhite AC and Evans KC (1985) Wave–wave interactions, microseisms, and infrasonic ambient noise in the ocean. *Journal of the Acoustical Society of America* 78: 981–994.

Nichols RH (1981) Infrasonic ambient ocean noise measurements: Eleuthera. *Journal of the Acoustical Society of America* 69: 974–981.

Sotrin BJ and Hodgkiss WS (1990) Fine-scale measurements of the vertical ambient noise field. *Journal of the Acoustical Society of America* 87: 2052–2063.

Urick RJ (1986) *Ambient Noise in the Sea*. Los Altos, CA, Peninsula Publishing.

Wenz GM (1962) Acoustic ambient noise in the ocean: spectra and sources. *Journal of the Acoustical Society of America* 34: 1936–1955.

ACOUSTIC SCATTERING BY MARINE ORGANISMS

K. G. Foote, Woods Hole Oceanographic Institution, Woods Hole, Massachusetts, USA

doi:10.1006/rwos.2001.0311

Historical Overview

Development of underwater sonar as a tool for navigation and military operations, following sinking of the *Titanic* in 1912, led inevitably to applications to marine organisms. By the 1930s, echoes from fish schools had been detected. In the 1940s, the deep sound-scattering layer was observed. Its biological origin in mesopelagic fish was identified in the 1950s. At the same time, applications to commercial fish were pursued with vigor, and both scientific echo sounders and fishery echo sounders began to be manufactured.

Steady improvements in transduction enabled individual fish of certain species and sizes to be detected at ranges of hundreds of meters. The ultrasonic frequency of 38 kHz was becoming a standard at this time; it was subsequently shown to be near the optimum for achieving detection of commercially important fish in the presence of attenuation due to spherical spreading and absorption. Parallel to studies of single-fish scattering at ultrasonic frequencies were studies of scattering at sonic frequencies, especially to determine the resonance frequency in swimbladder-bearing fish, which is a measure of size.

Echo integration was introduced in 1965 as a tool for quantifying fish aggregations at essentially arbitrary conditions of numerical density. This was rapidly developed, and it has been used routinely in surveys of fish stock abundance since about 1975. Introduction of standard-target calibration in the early 1980s served the cause of quantification by providing a rapid, high-accuracy method of enabling the results of echo integration to be expressed in absolute physical units. With few exceptions, standard-target calibration has become the method of choice.

Sonar, with one or more obliquely oriented or steerable beams, began to find common application in the 1970s for counting fish schools that might be missed by a vertical echo sounder beam. This was a significant development for acknowledging the narrowness of the sampling volume of vertically oriented directional echo sounder beams and the possibility of fish avoidance reactions to the transducer platform, typically a research vessel.

In another parallel development, the Doppler principle was exploited to measure the rate of approach or recession of fish targets. Both horizontally oriented echo sounder beams and sonar beams were used. Early applications determined the swimming speeds of schools of small pelagic fish and individual salmon in rivers.

Applications of acoustics to fish in the 1970s were accompanied by notable applications to zooplankton, if pursued less intensively owing to differences in commercial importance. Because of the enormous diversity of zooplankton species in size, shape, and composition, it was recognized early that insonification over a band of frequencies is